

Machine Learning guided high-throughput search of non-oxide garnets

Jonathan Schmidt,¹ Hai-Chen Wang,¹ Georg Schmidt,¹ and Miguel A. L. Marques^{1,*}

¹*Institut für Physik, Martin-Luther-Universität Halle-Wittenberg, D-06099 Halle, Germany*

Garnets, known since the early stages of human civilization, have found important applications in modern technologies including magnetorestriction, spintronics, lithium batteries, etc. The overwhelming majority of experimentally known garnets are oxides, while explorations (experimental or theoretical) for the rest of the chemical space have been limited in scope. A key issue is that the garnet structure has a large primitive unit cell, requiring an enormous amount of computational resources. To perform a comprehensive search of the complete chemical space for new garnets, we combine recent progress in graph neural networks with high-throughput calculations. We apply the machine learning model to identify the potential (meta-)stable garnet systems before systematic density-functional calculations to validate the predictions. In this way, we discover more than 600 ternary garnets with distances to the convex hull below 100 meV/atom with a variety of physical and chemical properties. This includes sulfide, nitride and halide garnets. For these, we analyze the electronic structure and discuss the connection between the value of the electronic band gap and charge balance.

I. INTRODUCTION

Garnets can be found throughout the world in diverse geological environments, and have been known since pre-history mainly due to their use in jewelry as gemstones. They are also relatively hard minerals, a property that makes them useful for a series of industrial applications, such as in waterjet cutting or as abrasives.

Generally, the garnets crystallize in a cubic structure (space group $Ia\bar{3}d$) with chemical composition $A_3B_2(B'C_4)_3$, where the A atoms are located in the 24c dodecahedral sites, the B atoms are in the 16a octahedral, and B' atoms occupy the 24d tetrahedral sites. In ternary garnets, B and B' sites are occupied by the same chemical element. Around 1950 [1–3] some rare-earth garnets, especially yttrium-based materials, started to attract attention. Those garnets have a general formula of $RE_3B_2(BO_4)_3$ where RE stands for rare-earth and B is a 3d magnetic transition metal (usually iron) or a group IIIA element. Among these, one of the most used ones is yttrium aluminum garnet (YAG), $Y_3Al_2(AlO_4)_3$, used as a synthetic simulant to diamond due to its high refractive index (> 1.8) [4]. Doped YAGs with other rare-earth elements have found numerous applications as lasing media in modern medical laser devices [5] or in tunable optical devices [6–9].

Other important compounds, with interesting ferri-magnetic properties, are the rare-earth iron garnets ($RE_3Fe_2(FeO_4)_3$, RIG). In the RIG structure, five Fe atoms occupy two different sublattices, and the anti-ferromagnetic coupling between sub-lattices and ferro-magnetic coupling within the sublattice leads to a ferri-magnetic configuration. RIGs can display a rather high Curie temperature (around 560 K [10]), and some systems exhibit giant magnetorestriction [11]. Moreover, RIGs materials have a band gap with values around 2.6

to 2.9 eV [12, 13]. Among these materials yttrium iron garnet (YIG) stands out because it has an exceptionally low Gilbert damping. YIG has first been used as bulk material in optical insulators, circulators and Faraday rotators. Since the last two decades, YIG is also more and more frequently used as thin film material for spintronic applications [14] because it allows the transmission of spin currents although being an insulator by itself. In recent years we have witnessed the attempt to replace yttrium by lanthanides to increase the spin orbit coupling and introduce even Dzyaloshinskii–Moriya interactions in hybrid systems.

Another interesting group of quaternary garnets is the lithium garnets $LN_3M_2(LiO_4)_3$, where LN is a lanthanide and M is either Te, Ta, or Nb. With partial Li-filling of the invasive positions of tetrahedral and distorted octahedral sites, the stuffed lithium garnets ($LN_3M_2Li_2(LiO_4)_3$) have a promising lithium-ion conductivity and chemical stability, showing potential as solid electrolytes in Li-batteries [15, 16].

The many applications of garnets, and of YIG in particular, has increased the need for garnets with different properties. Unfortunately the deposition of garnet thin films with high quality is only possible on garnet substrates due to the special crystal structure [17–19]. Moreover for spintronics applications it would be a huge step forward to be able to pair, for example, thin YIG films in hybrid structures with other conducting films being either metallic or having such a low band gap that reasonable electron conductivity is achievable at room temperature [17–19]. Again to achieve a perfect interface in these structures one would need to create an all-garnet hybrid which is currently prevented by the obvious lack of room temperature conducting or metallic garnets. Such a material class would dramatically extend the applicability of garnet thin films.

However, despite these diverse applications and the technological relevance of garnets, most of the research in garnets is confined to oxides [20], and only a few halides (also called cryolithionites) are known experi-

* miguel.marques@physik.uni-halle.de

mentally [21]. This is can be easily understood, as oxides are usually simpler to work with under ambient experimental conditions. Furthermore, a computational high-throughput search of new compositions for the garnet prototype is challenging, as the garnet cubic primitive unit cell contains 80 atoms, which is an order of magnitude larger than most structure prototypes used in recent high-throughput searches such as (double-)perovskites [22, 23], (half)-Heuslers [24], dichalcogenides [25], etc.

Fortunately, with the aid from state-of-the-art machine learning techniques, the problem of searching through the entire combinatorial chemical space can be significantly accelerated. With pre-trained machine models, we can filter millions of compositions according to the predicted stability without performing costly density functional theory (DFT) calculations for all the compositions. Nevertheless, DFT validation of the stable compounds is still necessary as a post-processing step.

In the present paper, we followed such a procedure to explore possible (meta-)stable compounds beyond oxy-garnets. The rest of the paper is structured as follows. In section II we explain the machine learning model and the computational methods we applied. In section III we present the most interesting crystal phases we uncovered in our work and discuss the potential applications of the new proposed compounds. Finally we present our conclusions and an outlook.

II. METHODS

A. Machine Learning Model

In this work we applied crystal graph attention networks, developed and pretrained in Ref. 22, to predict thermodynamically stable materials. The networks use an attention-based message passing approach based on the crystal graph representation of the crystal structure. Replacing the normal distance information that is typically used as edge-representation in crystal graph networks with solely the graph distance of the atoms to their neighbors allows for precise predictions of unrelaxed structures. As garnets crystallize in a cubic structure the list of neighbors and consequently the graph distances are mostly constant throughout the geometry relaxation. This removes the need to perform predictions with multiple cell constant ratios.

We study all garnet compositions $A_3B_5C_{12}$ considering all elements up to Bi, excluding only the rare-gases, and spanning a space of around 550k possible compounds. Obviously, most of these hypothetical compounds are highly unstable from the thermodynamic point of view. As discussed in Ref. [22], current machine learning approaches for the prediction of thermodynamic stability suffer from a considerable error due to the strong bias present in the existing datasets. To circumvent this problem, we use the following work-

flow: (i) The machine-learning model is used to predict the distance to the convex hull of stability for all 550k compounds. At the start we use the pre-trained machine from Ref. [22]; (ii) We perform DFT geometry optimizations to validate all compounds predicted below 200 meV/atom from the hull; (iii) We add these calculations to a dataset containing all DFT calculations for garnet systems. (iv) We use transfer learning to train a new model using this dataset with a training/validation/testing split of 80%/10%/10%. (v) The cycle is restarted.

In total we repeated the cycle three times. In the first, we performed DFT calculations for 3320 compounds. The mean absolute error (MAE) of the initial pre-trained machine was 0.497 eV/atom. This is a very high value, that was expected as there were very few garnets in the dataset used in Ref. [22], and they spanned a very small chemical space. In the second cycle we validated 7336 compounds, and the transfer-learning model performed much better, with a MAE of 0.064 eV/atom. Finally, in the third cycle we computed 3844 materials with DFT. The final model had a MAE of 0.058 eV/atom, showing that the transfer-learning workflow is meaningful and converges quickly.

B. DFT Calculations

We perform DFT calculations using the package VASP with PAW [26] datasets of version 5.2. and with the Perdew-Burke-Ernzerhof [27] (PBE) exchange-correlation functional. Following the Materials Project [28] recommendations, we use extra on-site corrections for oxides, fluorides containing Co, Cr, Fe, Mn, Mo, Ni, V, and W. The on-site corrections are repulsive and correct the d-states by respectively 3.32, 3.7, 5.3, 3.9, 4.38, 6.2, 3.25, and 6.2 eV. A cutoff of 520 eV is applied to the planewaves, and Γ -centered k -point grids with a uniform density of 1000 k-points per reciprocal atom are used to sample the Brillouin zone. For geometry optimizations all forces are converged to less than 0.005 eV/Å.

All calculations are performed with spin-polarization, starting from a ferromagnetic ground-state as is customary in high-throughput searches. Unfortunately, this means that, in most cases, antiferromagnetic or ferrimagnetic systems will converge to an incorrect ferromagnetic ground-state. This is important, in our context, particularly for ferrimagnetic garnets having a 3d transition metal such as Fe, Ni, Co, Cr, Mn, or V in the B position. We note that not only the spin-state of these garnets but also of anti- and ferrimagnetic systems on the convex hull are treated incorrectly. Consequently, the estimation of E_{hull} for ferrimagnetic garnets is far less accurate than for non-magnetic ones. For example, the experimentally known $\text{Gd}_3\text{Fe}_5\text{O}_{12}$ is predicted to be more than 1 eV above the hull according to Materials Project database [28], a value that is certainly grossly overestimated.

TABLE I: Number(meta-)stable systems (N_{stable}) below 100 meV/atom from the convex hull of thermodynamic stability and high-throughput success rate (R) for each category.

Category	N_{stable}	R (%)
Sulfides	70	14
Selenides	68	15
Tellurides	28	7
Nitrides	64	35
Fluorides	62	17
Chlorides	68	16
Bromides	72	17
Iodides	68	15
Hydrides	69	8
Total	569	14

To properly estimate E_{hull} for the ferrimagnetic garnets would require obtaining the correct magnetic ordering for a portion of the convex hull as well as for the garnets. This is a complex and computationally expensive task, that is well beyond the scope of this work. Therefore, we made the choice to restrict our discussion to systems not containing the 3d metals mentioned above in the B-site.

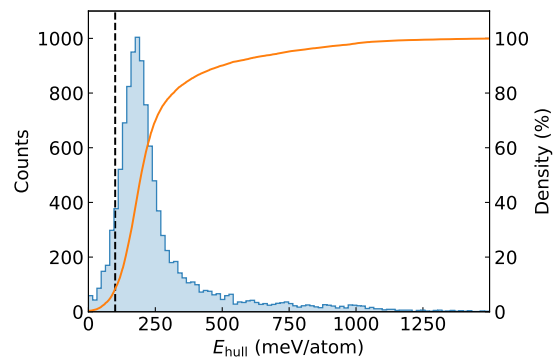
It is well-known that the electronic band gaps calculated with the PBE functional are severely underestimated [29]. Therefore, to obtain a more reliable estimation of this important physical property we performed calculations with the modified Becke-Johnson (mBJ) approximation [30], as this is by now recognized as one of the most accurate functionals for this task [31].

To calculate the averaged carrier effective masses from the interpolated eigenvalues we follow the approach of Ref. [32]. Considering a temperature of 300 K, we deduce the chemical potential required to reach a reference carrier concentration (10^{18} cm^{-3}) by using BOLTZTRAP2. We use a k -point mesh with a regular density of 2000 k -points per reciprocal atom and interpolated the calculated eigenvalues using BOLTZTRAP2 [33, 34]. The calculated averaged carrier effective masses can be seen as the intrinsic tendency for creating mobile charge carriers in materials [32].

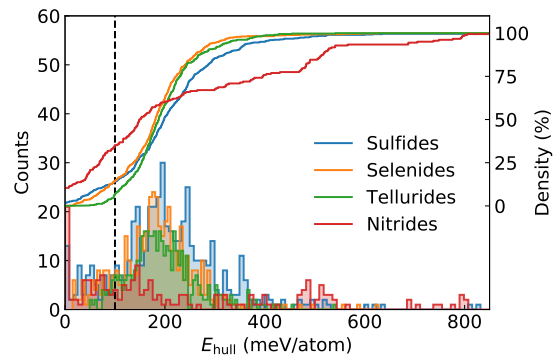
III. RESULTS AND DISCUSSION

A. Stability and Chemistry

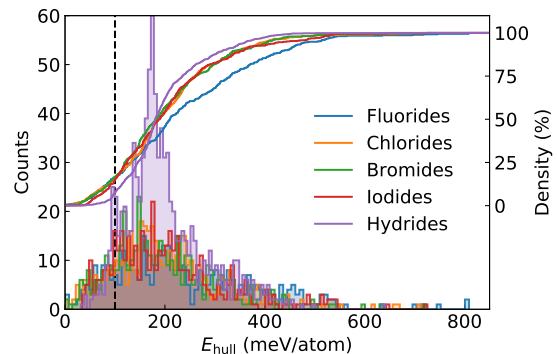
In total the machine-learning model predicted around 12300 compositions below 200 meV/atom from the convex hull of thermodynamic stability that were not present in the Materials Project database [28] nor in the Inorganic Crystal Structure Database [35] (ICSD). All these calculations can be downloaded from the Materials Cloud



(a)



(b)



(c)

FIG. 1: The distribution of the distance to the convex hull (E_{hull}) for (a) all calculated compositions, (b) halides, and (c) chalcogenides/nitrides. The cutoff to filter (meta-)stable systems (100 meV/atom) is shown as dashed vertical line.

repository [36].

After the DFT validation calculations we re-evaluated the distance to the convex hull (E_{hull}) of these candidates using the much more complete convex hull of Ref. [22]. The histogram of the values E_{hull} is shown in Fig. 1a. We also separate the systems into sulfides, selenides, tellurides, nitrides, chlorides, bromides, iodides, and hydrides. These comprise the majority of all systems

found. Most of the candidates have an E_{hull} larger than 100 meV/atom, but there are still more than one thousand (about 9%) compositions below this threshold. The high-throughput success rate, that we define by the number of compounds that are within 100 meV/atom from the convex hull divided by the total number of DFT calculations, stood at 14%, with a maximum of 35% for nitrides and a minimum of 8% for hydrides. These numbers prove the efficiency of our machine-learning assisted high-throughput search. The histogram of E_{hull} for these categories as well as all calculated compositions are shown in Fig. 1.

The distribution of E_{hull} for all systems follows the typical skewed Gaussian with the peak located at around 200 meV/atom and a fat tail that extends beyond 1 eV/atom, in agreement with the MAE errors for our machine-learning models. Individual distributions for chalcogenides are also skewed Gaussians peaking at around 200 meV/atom. The amount of (meta-)stable compounds decreases from sulfides to tellurides, which is also expected as this is the common trend of stability for the chalcogenides. Unlike the situation for chalcogenides, the distribution curve for nitrides has multiple peaks, and shows that there are plenty of potentially stable nitride garnets. For halides and hydrides the histograms are again skewed Gaussian similar to those of chalcogenides, but there is no clear trend in what concerns stability across the group. For hydrides, the total number of systems is much larger, but a lower percentage of them are (meta-)stable compared to the halides.

The total number of (quasi-)stable systems for each category is listed as Table I. A full list of the systems can be found in Table 1 of the Supplementary Information (SI). We also selected a dozen of them to analyze more closely in Table III. Later discussions will mainly focus on these systems.

From our calculations we recover the majority of the oxide (and halide) garnets that are already known experimentally, but we also obtain a wealth of different compounds not present in available databases. Many of these systems are oxides, that have been the subject of a recent high-throughput search [20] with results similar to ours. Interestingly, we also find a wealth of other chalcogenides, nitrides, halides, and even hydrides as shown in Figs. 1b,1c and in Table I.

From the stable compounds, several are closely related to the oxide garnets by the chemical substitution of oxygen by another chalcogen. These garnets along with their counterparts are presented in Table II. The existence of such compounds is expected due to the chemical similarity among chalcogens. In those chalcogenides, the dodecahedral sites (site A in $A_3B_5S_{12}$) are mostly occupied by rare earth elements, and according to the element occupying the octahedral and tetrahedral sites (site B), the chalcogenides can be further divided into several categories. The numbers of (meta-)stable systems for each category decrease in the following order: occupying B with group IIIA elements (Al, Ga, In, Tl), group IVA

elements (Ge, Sn, Pb), group VA elements (As, Sb, Bi), and transition metals (Ag, Cu, Sc, Ti). The preference of group IIIA elements for site B can be understood by simple charge compensation arguments. The most common oxidation state of the chalcogens is -2 , while the rare earth elements in sites A are $+3$: the composition reaches the “balanced” or “compensated” state if B is in the oxidation state $+3$. Moreover, for balanced $A_3^{\text{III}}B_5^{\text{III}}C_{12}^{\text{II}}$ chalcogenide compositions, one would expect the compounds to be semiconductors. This is indeed what we find (see an example in section III B).

Besides the chalcogenides, we discover 64 stable nitrides as seen in Table I. As discussed above, to reach a balanced oxidation state, elements with higher oxidation state should be favored to combine with -3 oxidation state of nitrogen. Indeed for nitride garnets $A_3B_5N_{12}$, the position A is mostly occupied by $+2$ or $+3$ chemical elements, and for position B the majority of meta-stable systems have elements with oxidation state $+6$ (Mo and W). Although a $+6$ element is required to achieve a balanced state, we also find that relatively stable compounds are possible for $+5$ (Nb and Ta), and $+7$ (Re). We could argue that the balanced nitrides should be semiconducting. However, due to the low electronegativity of nitrogen the gap may close (see one such example in section III B).

We can also identify several halides and hydrides from Figure 1c. However, halogens (and hydrogen in hydrides) have an oxidation state of -1 , which makes it more difficult to reach a balanced oxidation state with the $A_3B_5C_{12}$ stoichiometry. One viable scheme is with an A element that is $+1$, while the B elements in $16a$ and $24d$ Wyckoff positions are respectively $+1$ and $+3$, i.e. having the form of $A_3^{\text{I}}B_2^{\text{III}}(C_4^{\text{I}})_3$. Chemical elements exhibiting both $+1$ and $+3$ oxidation states are quite rare. Nevertheless, we still discovered some meta-stable semiconducting halide garnets, for example $K_3In_5F_{12}$.

There are other compositions that do not belong to any of the discussed classes, such as for example $Sr_{12}Zn_3H_5$. Most of them are “inverted”-garnets, i.e. with cations instead of anions occupying the C-sites, and have a comparatively higher E_{hull} than regular garnets. Furthermore, only a few anti-garnets with the A and B sites both occupied by the chemical elements of the nitrogen group could potentially become oxidation state balanced.

We have to again emphasize that, in order to form (meta-)stable or insulating/semiconducting compounds, charge compensation is neither a necessary nor a sufficient condition, and we find many exceptions in Table S1 in the Supplementary Information. However, it gives us a simple, intuitive argument to understand why a system is stabilized or has an electronic band gap. Furthermore, we have to keep in mind that uncompensated systems might be further stabilized through defects, such as vacancies. To simplify our discussion, we leave such possibilities to future works, and focus in the following on (meta-)stable regular garnets systems which could have balanced charges, specifically chalcogenides (except oxides), halides, hydrides, and nitrides.

TABLE II: The experimentally known oxy-garnets (not including a 3d metal in the B site), their ICSD ID, Materials Project ID, and predicted meta-stable counterparts with different C anions. The distance to the hull calculated with DFT is in parentheses (in meV/atom).

Formula	ICSD ID	MP ID	Counterparts
Y ₃ Al ₅ O ₁₂	20090, 41144, 41145, 67102, 67103,	mp-3050	Y ₃ Al ₅ S ₁₂ (-4); Y ₃ Al ₅ Se ₁₂ (36); Y ₃ Al ₅ Te ₁₂ (84)
	93634, 93635, 170157, 170158, 236589,		
	280104, 17687, 17688, 17689, 17690,		
	74607, 31496		
La ₃ Al ₅ O ₁₂		mp-780432	La ₃ Al ₅ S ₁₂ (-4); La ₃ Al ₅ Se ₁₂ (19); La ₃ Al ₅ Te ₁₂ (49)
Eu ₃ Al ₅ O ₁₂	245326	mp-21757	Eu ₃ Al ₅ S ₁₂ (39); Eu ₃ Al ₅ Se ₁₂ (93)
Tb ₃ Al ₅ O ₁₂	33602	mp-14387	Tb ₃ Al ₅ S ₁₂ (-4); Tb ₃ Al ₅ Se ₁₂ (29); Tb ₃ Al ₅ Te ₁₂ (79)
Er ₃ Al ₅ O ₁₂	170147, 280606, 170146, 62615	mp-3384	Er ₃ Al ₅ S ₁₂ (6); Er ₃ Al ₅ Se ₁₂ (50); Er ₃ Al ₅ Te ₁₂ (98)
Gd ₃ Al ₅ O ₁₂	192184	mp-14133	Gd ₃ Al ₅ S ₁₂ (-16); Gd ₃ Al ₅ Se ₁₂ (21); Gd ₃ Al ₅ Te ₁₂ (66)
Ho ₃ Al ₅ O ₁₂	409390, 33603	mp-14388	Ho ₃ Al ₅ S ₁₂ (-1); Ho ₃ Al ₅ Se ₁₂ (44); Ho ₃ Al ₅ Te ₁₂ (92)
Lu ₃ Al ₅ O ₁₂	259144, 17789, 182354	mp-14132	Lu ₃ Al ₅ S ₁₂ (28); Lu ₃ Al ₅ Se ₁₂ (70)
Y ₃ Ga ₅ O ₁₂	80148, 14343, 185862, 23852	mp-5444	Y ₃ Ga ₅ S ₁₂ (47); Y ₃ Ga ₅ Se ₁₂ (81)
La ₃ Ga ₅ O ₁₂		mp-780561	La ₃ Ga ₅ S ₁₂ (36); La ₃ Ga ₅ Se ₁₂ (51); La ₃ Ga ₅ Te ₁₂ (100)
Tb ₃ Ga ₅ O ₁₂	20831, 84875, 184934	mp-5965	Tb ₃ Ga ₅ S ₁₂ (37); Tb ₃ Ga ₅ Se ₁₂ (75)
Sm ₃ Ga ₅ O ₁₂	9236, 84873, 291192	mp-5800	Sm ₃ Ga ₅ S ₁₂ (29); Sm ₃ Ga ₅ Se ₁₂ (64); Sm ₃ Ga ₅ Te ₁₂ (93)
Nd ₃ Ga ₅ O ₁₂	84872	mp-15239	Nd ₃ Ga ₅ S ₁₂ (26); Nd ₃ Ga ₅ Se ₁₂ (54); Nd ₃ Ga ₅ Te ₁₂ (96)
Gd ₃ Ga ₅ O ₁₂	9237, 37145, 192181, 84874, 184931	mp-2921	Gd ₃ Ga ₅ S ₁₂ (32); Gd ₃ Ga ₅ Se ₁₂ (67); Gd ₃ Ga ₅ Te ₁₂ (93)
Lu ₃ Ga ₅ O ₁₂	23850	mp-14134	Lu ₃ Ga ₅ S ₁₂ (74)
Dy ₃ Ga ₅ O ₁₂	409391	mp-15576	Dy ₃ Ga ₅ S ₁₂ (49); Dy ₃ Ga ₅ Se ₁₂ (81)
Er ₃ Ga ₅ O ₁₂	9238	mp-12236	Er ₃ Ga ₅ S ₁₂ (55); Er ₃ Ga ₅ Se ₁₂ (95)
Ho ₃ Ga ₅ O ₁₂	409390	mp-15575	Ho ₃ Ga ₅ S ₁₂ (52); Gd ₃ Ga ₅ Se ₁₂ (89)

TABLE III: The calculated lattice constant (a , in Å), band gap calculated with PBE (Gap^{PBE}) and MBJ (Gap^{MBJ}) functional (in unit of eV), distance to the convex hull (E_{hull} in meV/atom), effective electron (m_e^*) and hole (m_h^*) masses (in unit of m_e^0), for some selected (meta-)stable sulfide and nitride garnets, data for Y₃Al₅O₁₂ is also listed for comparison.

Formula	a	Gap^{PBE}	Gap^{MBJ}	E_{hull}	m_e^*	m_h^*
Y ₃ Al ₅ O ₁₂	12.125	4.53	6.12	0	1.3	6.8
Y ₃ Al ₅ S ₁₂	14.932	2.08	3.00	0	0.7	1.5
Y ₃ Ga ₅ S ₁₂	15.073	1.32	2.45	46	0.5	3.2
Y ₃ In ₅ S ₁₂	15.709	1.35	2.38	46	0.5	2.6
Y ₃ Al ₅ Se ₁₂	15.752	1.46	2.15	36	0.5	1.5
Y ₃ Al ₅ Te ₁₂	17.120	0.60	1.07	84	0.3	2.7
Y ₃ Ge ₅ S ₁₂	15.324	0.00	0.00	81	-	-
Ca ₃ W ₅ N ₁₂	12.928	0.93	1.57	0	0.9	3.2
Ca ₃ Re ₅ N ₁₂	12.896	0.00	0.00	9	-	-
La ₃ Nb ₅ N ₁₂	13.297	0.00	0.00	99	-	-
K ₃ In ₅ F ₁₂	14.898	2.41	3.39	59	0.8	6.1
K ₃ In ₅ I ₁₂	19.977	0.00	0.00	61	-	-
Mg ₃ Rh ₅ H ₁₂	11.008	0.00	0.00	51	-	-
Y ₃ Rh ₅ H ₁₂	11.581	0.00	0.00	92	-	-

B. Electronic Structure

We illustrate the possible electronic structures of our garnets through a few selected examples depicted in Figs. 2–4.

Generally the electron states around the Fermi level in garnets can be classified in three categories: (i) from s-p, p-p, or even d-p bonding orbitals between B and C

atoms, (ii) from corresponding anti-bonding between B and C atoms, and, (iii) from d-electrons from A atoms if these are d-block or f-block metals. From the simplest tight-binding model, and as expected from $k \cdot p$ theory, we know that the larger the difference between the electronegativity of B and C and the shorter B–C bond-length, the larger the separations between states (i) and (ii). For the d (or f) block elements occupying the A-site, the position of states (iii) can be between (i) and (ii), overlapping with, or even above the latter. In charge compensated situations, the bands (i) are completely filled, while (ii) and (iii) (if applicable) bands are empty, resulting in insulating/semiconducting systems. Otherwise, depletion of bands (i) or filling of bands (ii) or (iii) can happen, leading to metallic systems. Although many deviations from this simple tight-binding picture appear, we will see how these general patterns are useful to understand the band-structures.

For chalcogenide garnets we chose as representative examples Y₃Al₅S₁₂, Y₃Ge₅S₁₂, and Y₃Ga₅S₁₂, while more examples can be found in the SI. The band-structures of these compounds are shown in Fig 2, together with Y₃Al₅O₁₂ for comparison. The oxidation-state balanced Y₃Al₅CH₁₂ (CH = S, Se, Te) garnets are semiconductors as expected. For Y₃Al₅S₁₂ the band structure is shown in Fig. 2b. Similar to its oxide counterpart in Fig. 2a, the Y–d states dominate the conduction bands (CB) slightly hybridizing with Al(p) and S(p)-states. These bands are from the type (iii) states as discussed above. The valence bands (VB) around Fermi level are mainly composed of the localized anionic p-states of type (i), also representing the typical situation described above. From

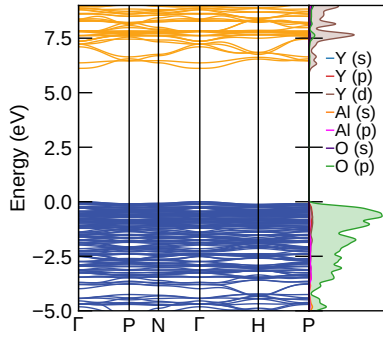
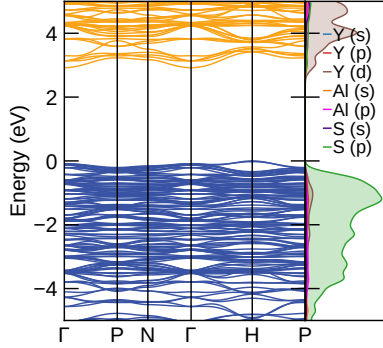
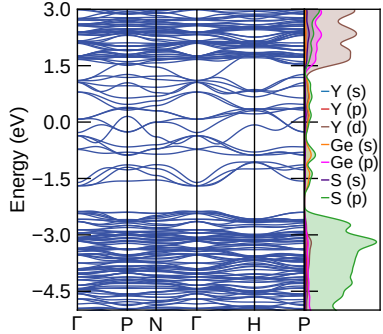
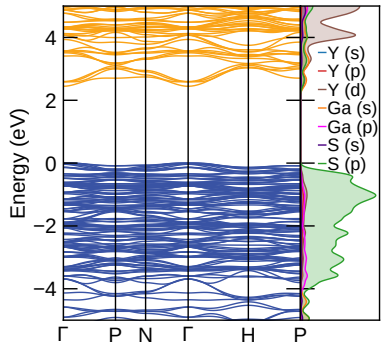
(a) $\text{Y}_3\text{Al}_5\text{O}_{12}$ (b) $\text{Y}_3\text{Al}_5\text{S}_{12}$ (c) $\text{Y}_3\text{Ge}_5\text{S}_{12}$ (d) $\text{Y}_3\text{Ga}_5\text{S}_{12}$

FIG. 2: Calculated mBJ electronic band structures for selected chalcogenide garnets. The Fermi level is set at zero.

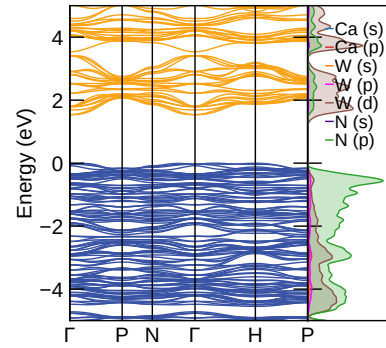
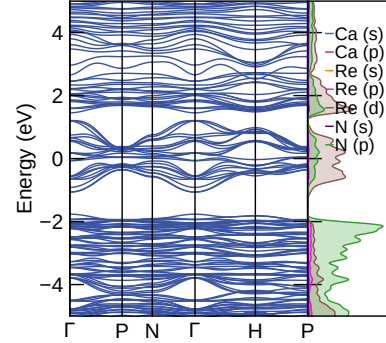
(a) $\text{Ca}_3\text{W}_5\text{N}_{12}$ (b) $\text{Ca}_3\text{Re}_5\text{N}_{12}$

FIG. 3: Calculated mBJ electronic band structures for selected nitride garnets. The Fermi level is set at zero.

$\text{Y}_3\text{Al}_5\text{O}_{12}$ to $\text{Y}_3\text{Al}_5\text{Te}_{12}$ (see Fig. S1 in SI), following the decreasing trend of electronegativity for chalcogens, the band gap shrinks and the band edges become more dispersed.

The elements occupying the B position in charge-compensated chalcogenides also have a crucial effect on the electronic structure. For example, $\text{Y}_3\text{B}_5\text{S}_{12}$ (B = Al, Ga, In, Tl, see Fig. S1 in the SI) all have a direct gap at Γ with the sole exception of $\text{Y}_3\text{Al}_5\text{S}_{12}$ which has an indirect $\text{H}-\Gamma$ gap. Moreover, going from Al to Tl the gap decreases, while the contribution of the s-states from the B atoms to the bottom of the conduction bands increases, leading to more extended bands and to lower effective electron masses. Furthermore, for $\text{Y}_3\text{Tl}_5\text{S}_{12}$ we can see that the Y(d) bands are above the Tl(s)-S(s) displaying more disperse anti-bonding mixing, an resulting in very low electron effective masses ($m_e^* = 0.19$).

For chalcogenides with unbalanced oxidation states, such as $\text{Y}_3\text{Ge}_5\text{S}_{12}$, similar features can also be observed (see Fig. 2c). Between the empty Y(d)-S(p) hybridization states of type (iii) and the full S(p) dominated type (i) bands are the states from Ge(s) and S(p) anti-bonding of type (ii). As discussed above they are partially occupied, so the system is metallic. It is possible that the system might re-establish a balanced oxidation state by creating Ge vacancies thus becoming semiconducting, though a detailed investigation of such a possibility is beyond the

scope of the present paper.

Some representatives of the band structures for nitrides garnets are shown in Fig. 3. The oxidation state compensated $\text{Ca}_3\text{W}_5\text{N}_{12}$ is semiconducting. The anti-bonding $p-d$ bands forming the CB separate also into two manifolds: the lower part is mainly constructed from the tungsten on the tetrahedral sites, and the upper part mainly from the octahedral W. The VB are, as usual, mostly composed of N(p) states. For charge unbalanced nitrides (such as $\text{Ca}_3\text{Re}_5\text{N}_{12}$) that have more valence electrons from Re compared to W, the Fermi level passes through the partially occupied $p-d$ anti-bonding bands and the system becomes metallic. However, the separation between $p-d$ bonding and anti-bonding bands can still be seen as well as the double manifolds of $p-d$ anti-bonding states. When a chemical element with less valence electrons replaces W, for example, in $\text{La}_3\text{Nb}_5\text{N}_{12}$ (see Fig. S1 in SI), the minority spin channel of $p-d$ bonding states is partially empty, and the system actually becomes a half-metal.

For halides, we show the band structure of $\text{K}_3\text{In}_5\text{F}_{12}$ and $\text{K}_3\text{In}_5\text{I}_{12}$ as examples. Apparently, the former compound has unbalance oxidation states, however it is semiconducting. The Bader net charges of the In at octahedral and tetrahedral sites are +1 and +2.4, respectively. The In in the B-site is therefore in the +1 and +3 oxidation states, reaching charge compensation as discussed above. The top of the valence bands are mainly composed of In(s)-F(p) anti-bonding states, which separate from the lower valence bands, formed by localized F(p)-In(p) bonding states, by around 4 eV. Unlike in most sulfides and nitrides, where d-states from A atoms dominate the bottom of the conduction bands, in $\text{K}_3\text{In}_5\text{F}_{12}$ the bottom of the CB is mainly formed by In(p)-F(p) anti-bonding hybridized states. This is because the K(s)-F(p) anti-bonding states have a much higher energy than d-p anti-bonding states in those sulfides and nitrides. When replacing F with I, the Bader net charges for the In atoms in octahedral and tetrahedral sites are respectively +0.7 and +1.0, showing that the +1/+3 oxidation states is not possible in $\text{K}_3\text{In}_5\text{I}_{12}$, and the system becomes metallic. The top valence band formed by In(p)-I(s) anti-bonding states separates in two manifolds. The upper part comes from the In atoms in tetrahedral sites and the lower belongs to the octahedral ones. This can be partially explained by the fact that the In-I bond length is larger in the latter.

In Fig 4 we show the band structure of selected examples of hydride garnets. For both $\text{Mg}_3\text{Rh}_5\text{H}_{12}$ and $\text{Y}_3\text{Rh}_5\text{H}_{12}$ the separation between H(s)-Rh(d) mixed bands and cation Rh(d) dominated bands are still present, similar to the situations in other uncompensated garnets. These two systems are also both charge uncompensated, the “extra” electrons partially filling the Rh(d) dominated bands, leading to metallic systems. Another way to re-establish compensation might be to force more H atoms to occupy the interstitial sites, but again, we leave exploration of this possibility to future investiga-

tions.

IV. CONCLUSIONS

We performed a machine-learning assisted high-throughput investigation of ternary garnets. We concentrated in non-oxides (that have been studied previously) and in ferromagnetic or paramagnetic compounds. We find a wealth of systems on the convex hull (i.e., thermodynamically stable) or close to it. This includes chalcogenides (with the stability decreasing from S to Te), nitrides, halides, hydrides, etc. We also found other possibilities, such as “inverted” garnets, but these were slightly less stable than the conventional phase. The materials tend to be semiconducting/insulating when the composition is charge compensated, otherwise we obtain metallic ground-states. The latter ones could be especially relevant as, to our knowledge, no garnets conducting at room temperature are known. Some of the metallic garnets even have lattice constants that are suitable to create hetero-structures with YIG.

A few chalcogenide garnets, in particular the sulfides, are thermodynamically stable, and are straightforward generalizations of common oxide garnets. Band-gaps are as expected considerably smaller for the sulfides, and decrease further across the periodic group. This opens up the possibility to engineer the band gap of garnets by anionic alloying, from the extreme ultraviolet of the oxide phase to UV-A regime or even into the visible. We predict several nitride systems that have interesting electronic properties due to the presence of transition metals in very high charge states. In view of the recent synthesis of two exotic nitride perovskites [37, 38] that were predicted [39, 40] with a method similar to the one used in this paper, we are confident that also nitride garnets are accessible experimentally. Finally, we find a few semiconducting halides where the chemical element occupying the octahedral and the dodecahedral site is in two different charge states.

Above all, we believe that our work proves that an exhaustive survey of the ternary, and perhaps also of the quaternary, space of materials is now accessible to high-throughput studies, even for large and complex unit cells. This is made possible by machine learning methods, that already achieved an outstanding maturity in the short time since their first appearance, and that are reaching an unprecedented accuracy. We expect these methods to further accelerate the discovery of new materials with exceptional properties.

V. ACKNOWLEDGEMENTS

The authors gratefully acknowledge the Gauss Centre for Supercomputing e.V. (www.gauss-centre.eu) for funding this project by providing computing time on the

- [1] HS Yoder and ML Keith, “Complete substitution of aluminum for silicon: The system $3\text{MnO}\cdot\text{Al}_2\text{O}_3\cdot 3\text{SiO}_2\text{—}3\text{Y}_2\text{O}_3\cdot 5\text{Al}_2\text{O}_3$,” *Am. Mineral.* **36**, 519–533 (1951).
- [2] F Bertaut and F Forrat, “Structure of ferrimagnetic rare-earth ferrites,” *CR Acad. Sci* **242**, 382 (1956).
- [3] R. C. LeCraw, E. G. Spencer, and C. S. Porter, “Ferromagnetic resonance line width in yttrium iron garnet single crystals,” *Phys. Rev.* **110**, 1311–1313 (1958).
- [4] ED Palik, in *Handbook of Optical Constants of Solids* (Elsevier, 1997).
- [5] Alexander Maninagat Luke, Simy Mathew, Maram Majeed Altawash, and Bayan Mohammed Madan, “Lasers: A review with their applications in oral medicine,” *J Lasers Med Sci.* **10**, 324 (2019).
- [6] M. Basavad, H. Shokrollahi, H. Ahmadvand, and S.M. Arab, “Structural, magnetic and magneto-optical properties of the bulk and thin film synthesized cerium- and praseodymium-doped yttrium iron garnet,” *Ceram. Int.* **46**, 12015–12022 (2020).
- [7] David Sedmidubský, Vít Jakeš, Kateřina Rubešová, Pavla Nekvindová, Tomáš Hlášek, Roman Yatskiv, and Pavel Novák, “Magnetism and optical properties of $\text{Yb}_3\text{Al}_5\text{O}_{12}$ hosted Er^{3+} – experiment and theory,” *J. Alloys Compd.* **810**, 151903 (2019).
- [8] A. H. Wako, F. B. Dejene, and H. C. Swart, “Effect of Ga^{3+} and Gd^{3+} ions substitution on the structural and optical properties of Ce^{3+} -doped yttrium aluminium garnet phosphor nanopowders,” *Luminescence* **31**, 1313–1320 (2016).
- [9] Jun Liu and Yogesh K. Vohra, “Sm:YAG optical pressure sensor to 180 GPa: calibration and structural disorder,” *Appl. Phys. Lett.* **64**, 3386–3388 (1994).
- [10] Vincent G. Harris, “Modern microwave ferrites,” *IEEE Trans. Magn.* **48**, 1075–1104 (2012).
- [11] F. Sayetat, “Huge magnetostriction in $\text{Tb}_3\text{Fe}_5\text{O}_{12}$, $\text{Dy}_3\text{Fe}_5\text{O}_{12}$, $\text{Ho}_3\text{Fe}_5\text{O}_{12}$, $\text{Er}_3\text{Fe}_5\text{O}_{12}$ garnets,” *J. Magn. Mater.* **58**, 334–346 (1986).
- [12] A. G. Gavriluk, V. V. Struzhkin, I. S. Lyubutin, and I. A. Trojan, “Irreversible electronic transition with possible metallization in $\text{Y}_3\text{Fe}_5\text{O}_{12}$ at high pressure,” *JETP Lett.* **82**, 603–608 (2005).
- [13] R. Metselaar and P.K. Larsen, “High-temperature electrical properties of yttrium iron garnet under varying oxygen pressures,” *Solid State Commun.* **15**, 291–294 (1974).
- [14] Mingzhong Wu and Axel Hoffmann, “Recent advances in magnetic insulators—from spintronics to microwave applications,” (2013).
- [15] Kannan Subramanian, George V. Alexander, K. Karthik, Srabani Patra, M.S. Indu, O.V. Sreejith, Raja Viswanathan, Janani Narayanasamy, and Ramaswamy Murugan, “A brief review of recent advances in garnet structured solid electrolyte based lithium metal batteries,” *J. Energy Storage* **33**, 102157 (2021).
- [16] Abin Kim, Seungjun Woo, Minseok Kang, Heetaek Park, and Byoungwoo Kang, “Research progresses of garnet-type solid electrolytes for developing all-solid-state li batteries,” *Front. Chem.* **8** (2020), 10.3389/fchem.2020.00468.
- [17] Georg Schmidt, Christoph Hauser, Philip Trempler, Maximilian Paleschke, and Evangelos Th. Papaioannou, “Ultra thin films of yttrium iron garnet with very low damping: A review,” *Phys. Status Solidi B* **257**, 1900644 (2020).
- [18] Matthias Althammer, “Pure spin currents in magnetically ordered insulator/normal metal heterostructures,” *J. Phys. D: Appl. Phys.* **51**, 313001 (2018).
- [19] A A Serga, A V Chumak, and B Hillebrands, “YIG magnonics,” *J. Phys. D: Appl. Phys.* **43**, 264002 (2010).
- [20] Weiye Ye, Chi Chen, Zhenbin Wang, Iek-Heng Chu, and Shyue Ping Ong, “Deep neural networks for accurate predictions of crystal stability,” *Nat. Commun.* **9** (2018), 10.1038/s41467-018-06322-x.
- [21] E. S. Grew, A. J. Locock, S. J. Mills, I. O. Galuskina, E. V. Galuskin, and U. Halenius, “Nomenclature of the garnet supergroup,” *Am. Mineral.* **98**, 785–811 (2013).
- [22] Jonathan Schmidt, Love Pettersson, Claudio Verdozzi, Silvana Botti, and Miguel A. L. Marques, “Crystal graph attention networks for the prediction of stable materials,” *Sci. Adv.* **7**, eabi7948 (2021).
- [23] Jonathan Schmidt, Jingming Shi, Pedro Borlido, Liming Chen, Silvana Botti, and Miguel A. L. Marques, “Predicting the thermodynamic stability of solids combining density functional theory and machine learning,” *Chem. Mater.* **29**, 5090–5103 (2017).
- [24] Anton O. Oliynyk, Erin Antono, Taylor D. Sparks, Leila Ghadbeigi, Michael W. Gaultois, Bryce Meredig, and Arthur Mar, “High-throughput machine-learning-driven synthesis of full-Heusler compounds,” *Chem. Mater.* **28**, 7324–7331 (2016).
- [25] Masahiro Fukuda, Jingning Zhang, Yung-Ting Lee, and Taisuke Ozaki, “A structure map for AB_2 type 2D materials using high-throughput DFT calculations,” *Mater. Adv.* **2**, 4392–4413 (2021).
- [26] P. E. Blöchl, “Projector augmented-wave method,” *Phys. Rev. B* **50**, 17953–17979 (1994).
- [27] John P. Perdew, Kieron Burke, and Matthias Ernzerhof, “Generalized gradient approximation made simple,” *Phys. Rev. Lett.* **77**, 3865 (1996).
- [28] Anubhav Jain, Shyue Ping Ong, Geoffroy Hautier, Wei Chen, William Davidson Richards, Stephen Dacek, Shreyas Cholia, Dan Gunter, David Skinner, Gerbrand Ceder, and Kristin a. Persson, “The materials project: A materials genome approach to accelerating materials innovation,” *APL Mater.* **1**, 011002 (2013).
- [29] Pedro Borlido, Thorsten Aull, Ahmad W. Huran, Fabien Tran, Miguel A. L. Marques, and Silvana Botti, “Large-scale benchmark of exchange–correlation functionals for the determination of electronic band gaps of solids,” *J. Chem. Theory Comput.* **15**, 5069–5079 (2019).
- [30] Fabien Tran and Peter Blaha, “Accurate band gaps of semiconductors and insulators with a semilocal exchange–correlation potential,” *Phys. Rev. Lett.* **102**, 226401 (2009).

- [31] Pedro Borlido, Jonathan Schmidt, Ahmad W. Huran, Fabien Tran, Miguel A. L. Marques, and Silvana Botti, “Exchange-correlation functionals for band gaps of solids: benchmark, reparametrization and machine learning,” *Npj Comput. Mater.* **6**, 96 (2020).
- [32] Geoffroy Hautier, Anna Miglio, Gerbrand Ceder, Gian-Marco Rignanese, and Xavier Gonze, “Identification and design principles of low hole effective mass p-type transparent conducting oxides,” *Nat. Commun.* **4** (2013), 10.1038/ncomms3292.
- [33] Georg K.H. Madsen and David J. Singh, “Boltztrap. a code for calculating band-structure dependent quantities,” *Comput. Phys. Commun.* **175**, 67 – 71 (2006).
- [34] Georg KH Madsen, Jesús Carrete, and Matthieu J Verstraete, “BoltzTraP2, a program for interpolating band structures and calculating semi-classical transport coefficients,” *Comput. Phys. Commun.* **231**, 140–145 (2018).
- [35] G. Gergerhoff F. H. Allen and R. Sievers, eds., *Crystallographic databases* (International Union of Crystallography, Chester, 1987).
- [36] Jonathan Schmidt, Hai-Chen Wang, Georg Schmidt, and Miguel A. L. Marques, “Machine learning guided high-throughput search of non-oxide garnets,” *Materials Cloud* (2022), 10.24435/materialscloud:gm-n0.
- [37] Kevin R. Talley, Craig L. Perkins, David R. Diercks, Geoff L. Brennecke, and Andriy Zakutayev, “Synthesis of LaWN₃ nitride perovskite with polar symmetry,” *Science* **374**, 1488–1491 (2021).
- [38] Simon D. Kloß, Martin L. Weidemann, and J. Paul Attfield, “Preparation of bulk-phase nitride perovskite LaReN₃ and topotactic reduction to LaNiO₂-type LaReN₂,” *Angew. Chem., Int. Ed.* **60**, 22260–22264 (2021).
- [39] Rafael Sarmiento-Pérez, Tiago F. T. Cerqueira, Sabine Körbel, Silvana Botti, and Miguel A. L. Marques, “Prediction of stable nitride perovskites,” *Chem. Mater.* **27**, 5957–5963 (2015).
- [40] José A Flores-Livas, R Sarmiento-Pérez, Silvana Botti, Stefan Goedecker, and Miguel A L Marques, “Rare-earth magnetic nitride perovskites,” *J. Phys.: Mater.* **2**, 025003 (2019).

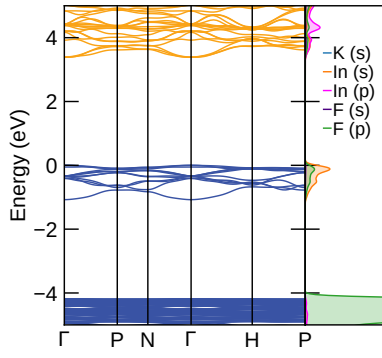
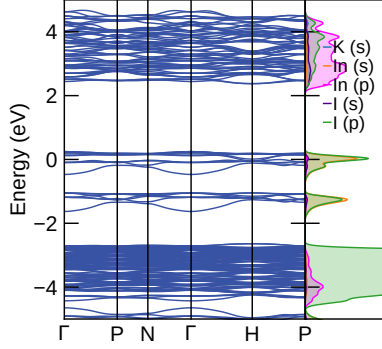
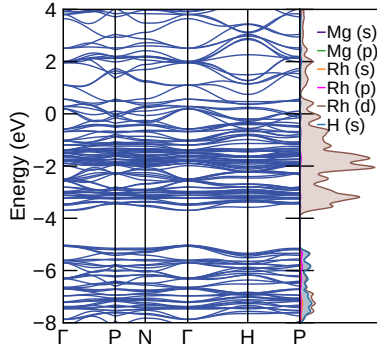
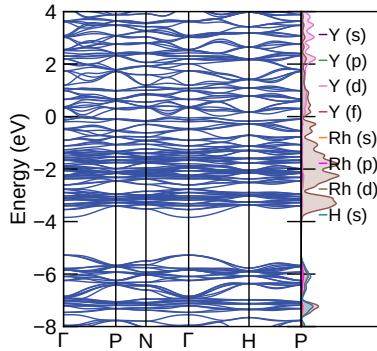
(a) $\text{K}_3\text{In}_5\text{F}_{12}$ (b) $\text{K}_3\text{In}_5\text{I}_{12}$ (c) $\text{Mg}_3\text{Rh}_5\text{H}_{12}$ (d) $\text{Y}_3\text{Rh}_5\text{H}_{12}$

FIG. 4: Calculated mBJ electronic band structures for selected halide and hydride garnets. The Fermi level is set at zero.